Available online at www.sciencedirect.com
ScienceDirect
International Journal of Thermal Sciences 48 (2009) 331–341
International Journal of Thermal Sciences
www.elsevier.com/locate/ijts

Flow boiling in a 1.1 mm tube with R134a: Experimental results and comparison with model

D. Shiferaw, T.G. Karayiannis *, D.B.R. Kenning

Brunel University, School of Engineering and Design, Uxbridge, West London, UB8 3PH, UK

Received 10 August 2007; received in revised form 25 February 2008; accepted 26 February 2008

Available online 18 April 2008

Abstract

A detailed comparison of flow boiling heat transfer results in a stainless steel tube of 1.1 mm internal diameter with results of a three-zone flow model are presented in this paper. The working fluid is R134a. Other parameters were varied in the range: mass flux 100–600 kg/m^2 s; heat flux 16–150 kW/m^2 and pressure 6–12 bar.

The experimental results demonstrate that the heat transfer coefficient increases with heat flux and system pressure, but does not change with vapour quality when the quality is less than about 50% for low heat and mass flux values. The effect of mass flux is observed to be insignificant. For vapour quality values greater than 50% and at high heat flux values, the heat transfer coefficient does not depend on heat flux and decreases with vapour quality. This could be caused by dryout. The three-zone evaporation model predicts the experimental results fairly well, especially at relatively low pressure. However, the dryout region observed at high quality is highly over-predicted by the model. The sensitivity of the performance of the model to the three optimised parameters (confined bubble frequency, initial film thickness and end film thickness) and some preliminary investigation relating the critical film thickness for dryout to measured tube roughness are also discussed.

Keywords: Flow boiling; Heat transfer; Two phase flow; Dryout; Roughness; Minichannel

1. Introduction

In recent years there has been increased research activity in flow boiling in very small diameter tubes and it is now highly desirable to develop mechanistic models for flow boiling in small to micro-channels that are well validated by experiments. Conventional ways of modelling boiling heat transfer coefficients in large channels are mainly based on empirical correlations and do not consider the effect of flow regime on heat transfer. Flow boiling heat transfer models have been proposed and are published in past papers, based on nucleate boiling, forced convective boiling, film flow boiling and annular two phase flow boiling. Experimental results for small diameter tubes also demonstrated heat transfer coefficients that were more or less independent of vapour quality and mass flux, but strongly dependent on heat flux and saturation pressure (Lazarek and Black [1], Wambsganss et al. [2], Tran et al. [3], Bao et al. [4], Palm [5], Huo et al. [6]). Conventionally, this is interpreted as evidence that nucleate boiling is the dominant heat transfer mechanism. However, using macroscale boiling heat transfer correlations and models based on the above premise did not predict well the heat transfer coefficient in small diameters, Qu and Mudawar [7], Owhaib and Palm [8] and Huo et al. [6].

Currently emerging flow regime based models provide a more realistic description of the various transport process from which important hydrodynamic and thermal parameters such as heat transfer and pressure drop can be derived. Recently, Thome et al. [9] proposed a model based on convective heat transfer in three zones within the confined bubble regime, without any contribution from nucleate boiling.

Most models, including the three-zone model, do not at present take fluctuations in saturation temperature into account. Yan and Kenning [10] showed that the pressure fluctuations were caused by the acceleration of liquid slugs by expanding confined bubbles, confirming a model of Kew and Cornwell [11], and that the corresponding fluctuations in saturation tem-

* Corresponding author.
E-mail address: tassos.karayiannis@brunel.ac.uk (T.G. Karayiannis).

1290-0729/$ – see front matter
doi:10.1016/j.ijthermalsci.2008.02.009

Nomenclature

Bo	Bond number $Bo = (\rho_l d/\sigma)U_p^2$	
$C_{\delta 0}$	correcting factor on the initial film thickness	
d	diameter	m
f	pair frequency	Hz
G	mass flux	kg/m^2 s
g	gravitational acceleration	m/s^2
h	enthalpy	J/kg
h_{lv}	latent heat of vaporisation	J/kg
L	length	m
m	mass flow rate	kg/s
P	pressure	Pa
Q	heat	W
q	heat flux	W/m^2
T	temperature	K
t	time	sec
U	velocity	m/s
x	thermodynamic quality	
z	axial distance	m

Greek symbols

α	heat transfer coefficient	W/(m^2 K)
Δ	finite increment	
δ	liquid film thickness	m
λ	thermal conductivity	W/m K
ν	kinematic viscosity	m^2/s
ρ	density	kg/m^3
σ	surface tension	N/m
τ	pair period	s

Subscripts

crit	critical
dry	dryout zone
dry film	dryout of liquid film
end	end
film	liquid film between bubble and wall
i	index
l	liquid
min	minimum
opt	optimum
p	pair
ref	reference
to	total
tp	two phase
v	vapour
w	wall
0	initial

perature were of similar magnitude to the mean superheat causing evaporation, so they could not be neglected. Zhang et al. [12,13] showed that the fluctuations in pressure, saturation temperature and wall temperature became more extreme for water boiling in microchannels with cross-sectional dimensions below 0.17 mm, so that they might influence mechanical integrity as well as thermal performance.

In channels of circular cross-section, in which events in the boiling region cannot be observed directly, decreases in time averaged heat transfer coefficient with increasing quality, often accompanied by fluctuating wall temperatures, have been attributed to transient dryout, particularly at low mass flux, and relatively high heat flux, Lin et al. [14], Yan and Lin [15], Huo et al. [6]. Wen et al. [16] observed at very low mass fluxes the downstream propagation of transient high wall temperatures indicative of dryout, even at low heat fluxes. Microchannel heat transfer correlations generally do not make allowance for transient dryout. However, the three-zone model includes a mechanism of periodic dryout.

Shiferaw et al. [17] compared the experimental results, obtained with two stainless steel tubes of internal diameter 4.26 and 2.01 mm using R134a at 8 bar and 12 bar system pressure, with the three-zone evaporation model for confined bubble flow proposed by Thome et al. [9]. Shiferaw et al. observed that the model predicted fairly well the experimental data that could have been previously interpreted as nucleate boiling due to their dependence on heat flux and independence of quality. However, it did not predict correctly the trends for changing diameter. Shiferaw et al. [17] also pointed out other features of the model that may require improvement. In the current paper the comparison is extended to heat transfer results for a 1.1 mm diameter tube, including high quality regions where partial dryout is deduced to occur.

The main features of the model, described briefly in Section 2, include three empirically determined constants, namely frequency of formation of confined bubbles, thickness of the thin film formed round a confined bubble and a critical value of the film thickness for dryout to occur, which is tentatively associated with the wall roughness.

2. Brief summary of the model

A brief review of the three-zone model developed by Thome and co-workers was presented in Shiferaw et al. [17] and is now included here for the sake of completeness. The full details are given in Thome et al. [9] and Dupont et al. [18]. The proposed model predicts the local dynamic and the local time-averaged heat transfer coefficient at fixed locations along the channel using an evaporation based model of the elongated bubble flow regime.

Fig. 1 illustrates the three-zone model. The model assumes the passage of a liquid slug followed by a confined elongated bubble trapping a thin liquid film against the inner wall, which means the existence of a pair consisting of the liquid slug and the elongated bubble. However, if the liquid film dries out by evaporation before the arrival of the next liquid slug, a vapour slug follows (triplet). The fact that the model considers a dryout zone and exploits the transient evaporation of the film is one of

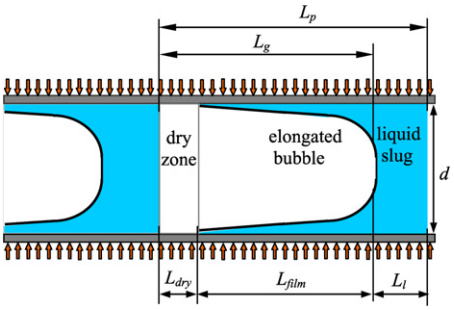

Fig. 1. Diagram illustrating the three zones: a liquid slug, an elongated bubble and a vapour slug, Thome et al. [9].

the novelties of the model. Nucleate boiling is not included in the model.

The time-averaged local heat transfer coefficient is determined by,

$$\alpha_{tp}(z) = \frac{t_l}{\tau}\alpha_l(z) + \frac{t_{film}}{\tau}\alpha_{film}(z) + \frac{t_{dry}}{\tau}\alpha_v(z) \tag{1}$$

The time periods used in the model are as follows: t_l corresponds to the time it takes for the liquid slug to pass a fixed location z through the cross section, $t_l = \tau/(1 + (\rho_l/\rho_v)(x/1-x))$; t_{film} is the residence time of the film; t_{dry} represents the duration of the local wall dryout; t_v corresponds to the presence of vapour (dryout and film zone) passing location z, $t_v = \tau/(1 + (\rho_v/\rho_l)(1-x)/x)$. The maximum duration, $t_{dry\ film}$, of the existence of the film at position z till dryout occurs at the minimum feasible film thickness (δ_{min}) is $t_{dry\ film}(z) = (\rho_l h_{lv}/q)(\delta_0(z) - \delta_{min})$. If $t_{dry\ film} < t_v$, local dryout occurs, i.e. the liquid film thickness reaches the minimum feasible film thickness, $\delta_{end}(z) = \delta_{min}$, and $t_{film} = t_{dry\ film}$ [9]. This implies that $t_{dry} = t_v - t_{film}$. On the other hand, if $t_{dry\ film} > t_v$, then no dryout occurs since the next liquid slug arrives before dryout of the film occurs and, $\delta_{end}(z) = \delta(z, t_v)$. In this case, $t_{film} = t_v$.

$\alpha_l(z)$ and $\alpha_v(z)$ are calculated from their local Nusselt numbers using the respective equivalent lengths L_l and L_{dry}, see Fig. 1. L_l and L_{dry} are the length of the liquid slug and dry wall zone, respectively. The London and Shah [19] correlation for laminar developing flow and the Gnielinski [20] correlation for transition and turbulent developing flow was recommended by Thome et al. [9]. The Churchill and Usagi [21] asymptotic method was used to obtain a continuous expression of the mean heat transfer coefficient as a function of Reynolds number.

The mean heat transfer coefficient through the evaporating thin liquid film surrounding the elongated bubble, $\alpha_{film}(z)$, was obtained as follows assuming one-dimensional heat conduction in a stagnant thin liquid film:

$$\alpha_{film}(z) = \frac{\lambda_1}{\delta_0 - \delta_{end}} \ln\left(\frac{\delta_0}{\delta_{end}}\right) \tag{2}$$

$$\delta(z,t) = \delta_0(z) - \frac{q}{\rho_l h_{lv}} t \tag{3}$$

$$\frac{\delta_0}{d} = C_{\delta 0}\left(3\sqrt{\frac{\nu_l}{U_p d}}\right)^{0.84}\left[(0.07Bo^{0.41})^{-8} + 0.1^{-8}\right]^{-1/8} \tag{4}$$

where

$$U_p = G_{tot}\left[\frac{x}{\rho_v} + \frac{1-x}{\rho_l}\right] \tag{5}$$

In the model, three parameters were not defined analytically, namely the minimum thickness of the liquid film at dryout (δ_{min}), the pair frequency (f), which is the frequency of the bubble generation and the correction factor, $C_{\delta 0}$ for the initial film thickness. Thome et al. recommended values of these parameters to be found by optimising the prediction of the model against an experimental database for the heat transfer coefficient. The initial thickness of the liquid film was found by using the Moriyama and Inoue [22] film thickness prediction and applying an empirical correction factor, $C_{\delta 0}$ as shown in Eq. (4). In Thome et al. [9], it was presented that the film thickness was governed by the evaporation of the liquid film. However, in Dupont et al. [18], where they compared the model predictions with a database (1591 test data for R11, R12, R113, R123, R134a, R141b and CO_2), they used a constant average film thickness. After optimising empirically each parameter with the whole range of the database, Dupont et al. recommended general values of the parameters as:

$$\delta_{min} = 0.3\ \mu m \tag{6}$$

$$f_{opt} = \left(\frac{q}{q_{ref}}\right)^{1.74}\ Hz \tag{7}$$

The reference heat flux (q_{ref}) was given as a function of the reduced pressure based on the method employed by Cooper [23] for the pool boiling correlation.

$$q_{ref} = 3328\left(\frac{P_{sat}}{P_{crit}}\right)^{-0.5} \tag{8}$$

The constant values of 3328 W/m^2 as well as the values of the exponents of Eqs. (7) and (8), i.e. 1.74 and −0.5, respectively were obtained from the complete experimental database (which included R134a). The constant in Eq. (4) was again obtained using the database as:

$$C_{\delta 0} = 0.29 \tag{9}$$

The local and average heat transfer coefficients that were used to compare with the results of the current experiments were calculated using the above recommended general values, Eqs. (6)–(9). However, it is desirable to obtain independent estimates of the three parameters from detailed observations.

3. Experimental facility and procedure

An experimental facility was constructed during the early part of this study to determine the heat transfer coefficient in small diameter tubes using R134a fluid. The experimental facility consists of three main systems, which are the R134a main circuit, data acquisition and control, and the R22 cooling system. The main facility, which is shown in Fig. 2, was designed to allow testing of different fluids and a wide range of flow conditions. Details of the experimental system were described in Huo et al. [6]. The test section was a stainless steel

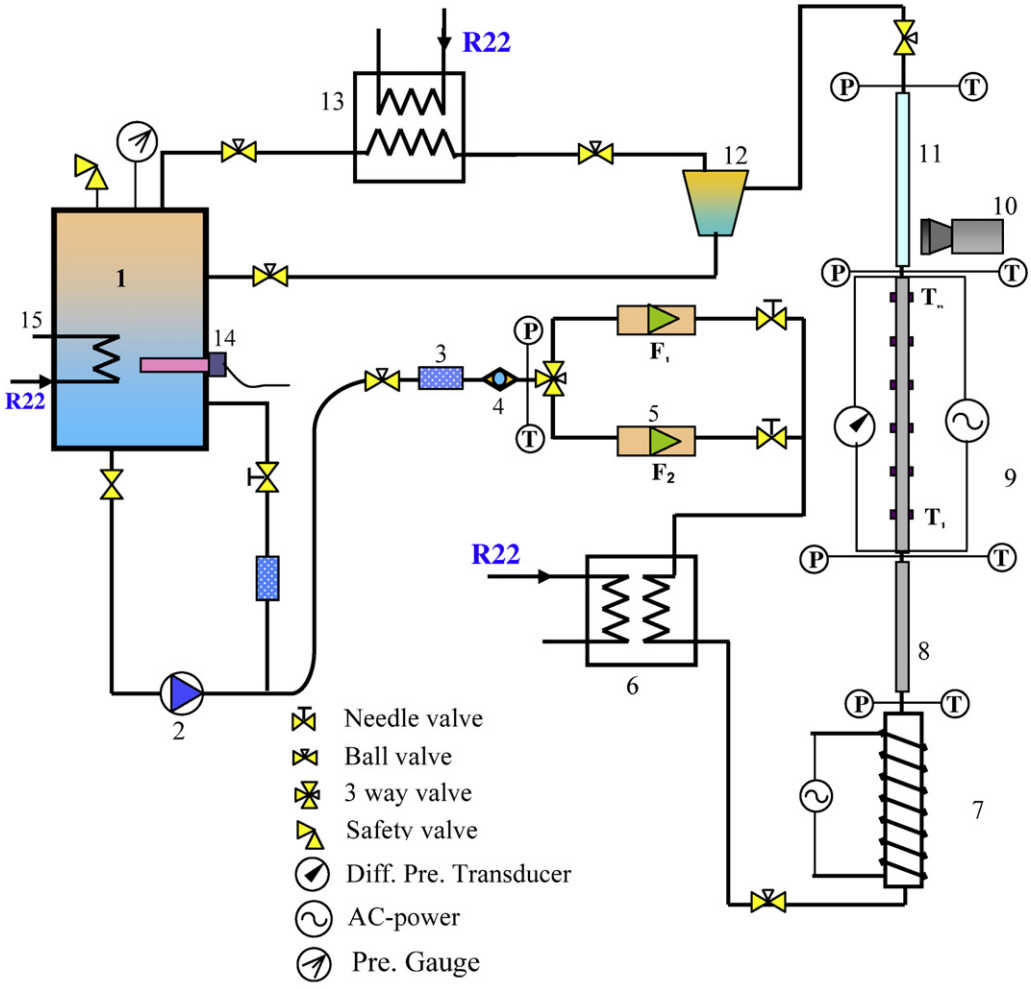

1	R134a reservoir	2	Pump	3	Filter Dryer
4	Sight glass	5	Flow meter	6	Subcooler
7	Preheater	8	Calming section	9	Heated test section
10	High-speed camera	11	Observation section	12	Separator
13	Condenser	14	Immersion heater	15	Cooling coil

Fig. 2. Schematic diagram of the flow patterns experimental system (the R22 Cooling system is not shown).

cold drawn tube of internal diameter 1.1 mm, heated length 150 mm, wall thickness 0.247 mm and roughness 1.28 μm. Direct electric heating was applied to the test section; fifteen K-type thermocouples were soldered to the outside of the tube at equal distances to provide the wall temperatures. The first and last thermocouple readings were not used in the analysis so as to avoid conduction errors. T-type thermocouples and pressure transducers were used to measure inlet and outlet temperatures and pressures. All the instruments used were carefully calibrated. The uncertainty in temperature measurement was ±0.2 K, flow rate measurements ±0.4%, and pressure measurements ±0.15%. A validation was performed using single phase pressure drop and heat transfer tests before running the boiling experiment. The single phase friction factor results agreed well with the Blasius correlation, i.e. within the uncertainty of the experiment. Also, the single phase Nusselt number (*Nu*) results agreed very well with the Dittus and Boelter [24] and Petukhov [25] correlations, again within the uncertainty limit. The results of these comparisons are given in Karayiannis et al. [26]. A series of flow boiling tests were performed at different mass flux and heat flux. In the heat transfer experiments, the fluid inlet temperature was kept slightly below saturation and the heat flux was increased in steps until the exit quality reached about 90% for a fixed mass flux and system pressure. The data were recorded after the system was steady, which normally took about 15 minutes but sometimes longer. Each recording was the average of 20 measurements. The next test was then performed at a different flow rate. A Pyrex glass tube for flow pattern observation was located immediately downstream of the heat transfer test section. A digital high-speed camera (Phantom V4 B/W, 250 × 512 pixels resolution, 2000 pictures/sec) was used

to observe the flow patterns. The results of the flow visualisation part of this study are presented in detail in Chen et al. [27].

The local heat transfer coefficient at each thermocouple point was determined based on the following equation:

$$\alpha = \frac{q}{T_w - T_l} \tag{10}$$

where T_w is the local inner wall temperature, T_l is the local fluid temperature and q is the inner wall heat flux to the fluid. T_l was deduced from the fluid pressure. This was determined based on the assumption of a linear pressure drop through the test section. T_w was calculated based on the outside surface temperature recorded by the thermocouples, heat flux and the tube wall thermal resistance using a one-dimensional conduction equation. The heat lost to the ambient, ΔQ, was included in the calculation. It was obtained from single-phase experiments conducted prior to each boiling test at the same condition. In all the cases, the heat loss was less than 1.4% of the input power. The average error in the heat transfer coefficient was ±6%. An energy balance based on the heat supplied minus losses and the enthalpy change enabled the exit thermodynamic quality to be calculated. The total enthalpy change across the test section was calculated based on the flow rate of the refrigerant and the pressure and temperature change measured by the differential pressure transducer and thermocouples, respectively, at two ends of the test section. The thermodynamic quality (x) was determined based on the heat transferred to the fluid, given as:

$$x_i = \frac{h_i - h_l}{h_{lv}} \tag{11}$$

where h_l and h_{lv} are the specific enthalpy of saturated liquid and latent heat of vaporisation, respectively. h_i is the local specific enthalpy of the fluid. This was determined from the enthalpy of the previous section and the heat transferred to the fluid, i.e.

$$h_i = h_{i-1} + \frac{L_i}{mL}(Q - \Delta Q) \tag{12}$$

where the heat input (Q) is equal to the product of the voltage and the current applied directly to the test section.

Reproducibility of the experimental data was tested frequently at different conditions. Fig. 3 shows the results of the repeatability tests, which were performed a few days and almost a year later. As seen in the figure, the differences in the results were mostly within the experimental error and hence reproducible.

The local flow boiling heat transfer coefficients for R134a were obtained for the range: pressure 6 to 12 bar, heat flux 16–170 kW/m^2, mass flux 100–600 kg/m^2 s, vapour quality 0–0.9.

4. Experimental results

Flow patterns were observed by the digital high-speed camera in a borosilicate glass tube with an internal diameter matched to the test section located immediately after the heated section and these are presented in Fig. 4. Fig. 4(a) shows typical flow patterns observed in this tube at different conditions, i.e. vapour and liquid superficial velocities, which were

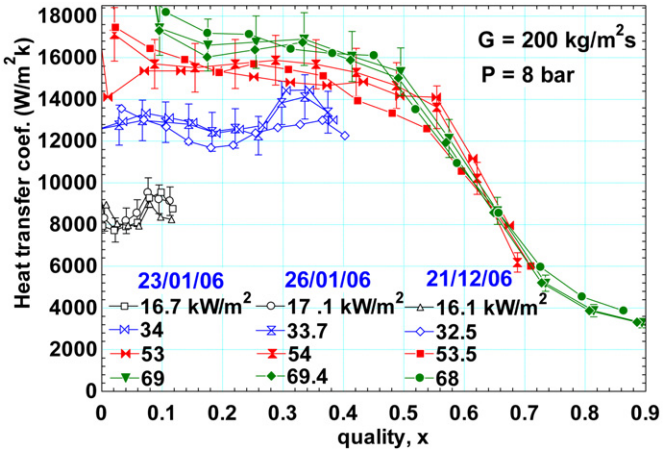

Fig. 3. Reproducibility of the experiments at a mass flux of 300 kg/m^2 s and 8 bar pressure.

reported in [27]. Chen et al. [27] studied tubes of 1.1, 2.01, 2.88 and 4.26 mm internal diameter and defined the regimes of dispersed bubble, bubbly, confined bubble, slug, churn, and annular flow. Dispersed bubble flow regime was found at very high mass flux condition and hence may not be observed during the present heat transfer studies, as these are low mass flux tests. They distinguished confined bubble flow (bubbles with convex rear ends) from slug flow (bullet shaped bubbles with sharp corners and a fluctuating surface at the rear) and noted that it first occurred for the 2.01 mm tube. These indications of the increasing importance of surface tension with decreasing diameter were consistent with the diameters predicted by the confinement number criterion. According to this criterion proposed by Cornwell and Kew [28] for small tube characteristics, confinement effects should be observed at diameter of tubes below 1.6 mm at 8 bar pressure, for R134a. This is roughly in agreement with Chen et al. and the present observation, since confined bubbles were observed at this (1.1 mm) tube. Fig. 4(b) shows flow pattern photographs at different heat flux for a mass flux of 200 kg/m^2 s and 8 bar pressure, taken simultaneously with the corresponding heat transfer tests presented hereinafter and show the prevailing flow regimes for the range presented in this paper. At low heat flux, confined bubble flow, comprising separated bubbles with size equivalent to tube internal diameter, is observed. As the heat flux increased, the bubbles grow in length and become elongated. Further increase in heat flux resulted in the liquid slug between the bubbles being pushed to the liquid film leaving a wavy annular film. A relatively uniform film is created when increasing the heat flux even further, reducing the wave irregularity. At high heat flux the annular flow pattern is observed, however the film interface is not quite smooth. Further discussion on the flow patterns in small/micro tubes is given in [26], where the case of a smaller tube of 0.52 mm is included.

The experimental local heat transfer coefficient is plotted as a function of quality in Figs. 5 and 6 for various heat fluxes. Fig. 5 shows some of the typical results at a mass flux of 200 kg/m^2 s and 8 bar system pressure. As seen in the figure, when $x < \sim 0.5$, the heat transfer coefficient depends on the

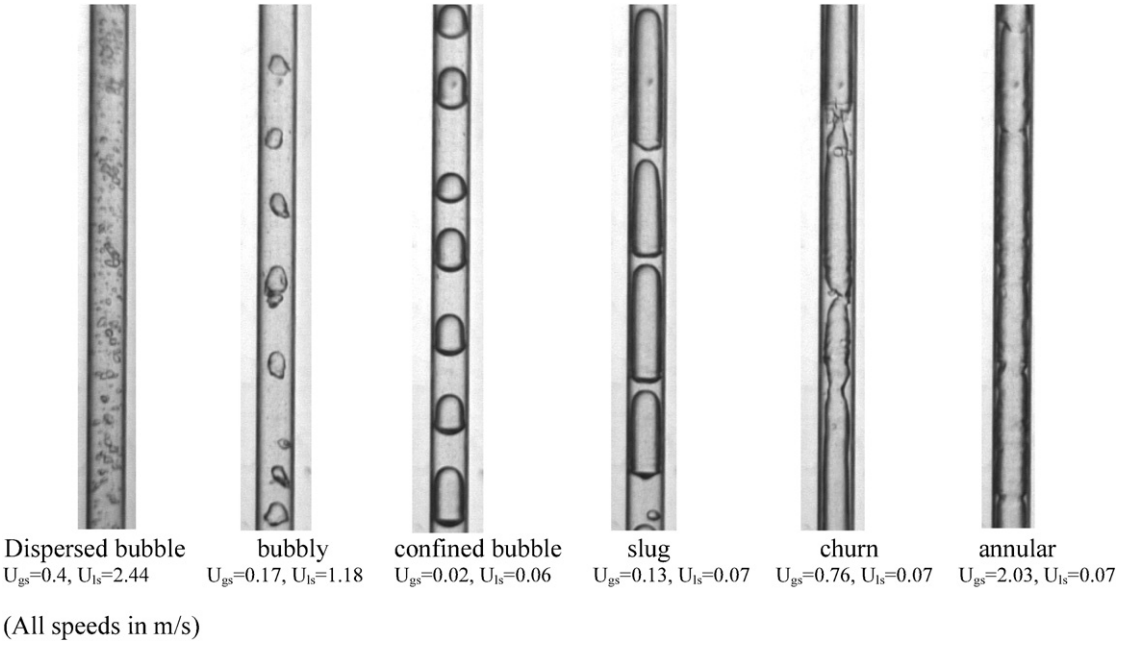

(a)

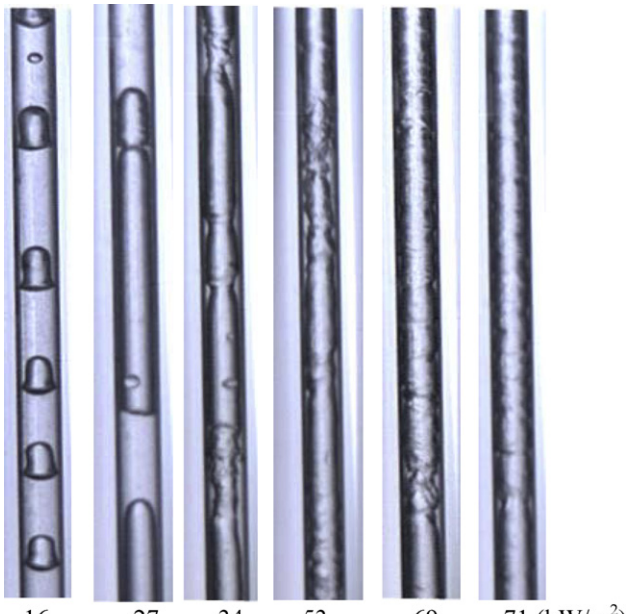

(b)

Fig. 4. Flow patterns observed (a) typical flow regimes at different conditions, [27], (b) typical patterns at a mass flux of 200 kg/m^2 s and 8 bar pressure corresponding to the heat transfer results presented in the paper.

heat flux and is almost independent of quality. At high values of heat flux and vapour quality greater than about 50%, the heat transfer coefficient becomes independent of heat flux and decreases monotonically with quality. At low values of heat flux (e.g., 16 and 27 kW/m^2), the heat transfer coefficient tends to depend on quality towards the exit of the test section.

At low mass flux, at which the heat transfer tests were conducted, transition to the annular flow pattern occurred at a relatively higher quality or heat flux. Besides, as the diameter decreases, confined bubble, slug, or churn flows become more typical flow patterns. The higher heat transfer coefficient at the front part of the test section may be caused by the relatively longer confined bubble/slug flow regimes, which are reported to be a better heat transfer regime with exit qualities low enough to avoid sustained dryout of the annular films around the bubbles [12,13]. A decrease in the heat transfer coefficient, which is observed towards the exit of the tube especially at high heat flux, could be related to the fact that annular flow is associated with film dryout and film waviness. Although the two phase flow patterns are created by directly heating the test section (unlike mixing gas/liquid), it is important to notice that these flow patterns are observed at an adiabatic section. Hence, the flow

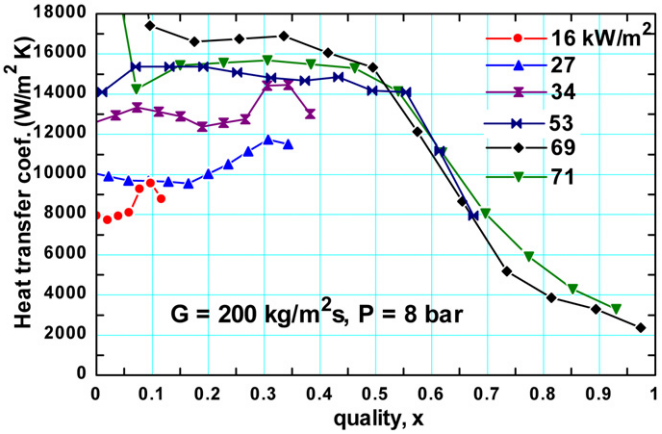

Fig. 5. Local heat transfer coefficient as a function of vapour quality with different heat fluxes; $G = 200$ kg/m^2 s, $P = 8$ bar at different heat flux.

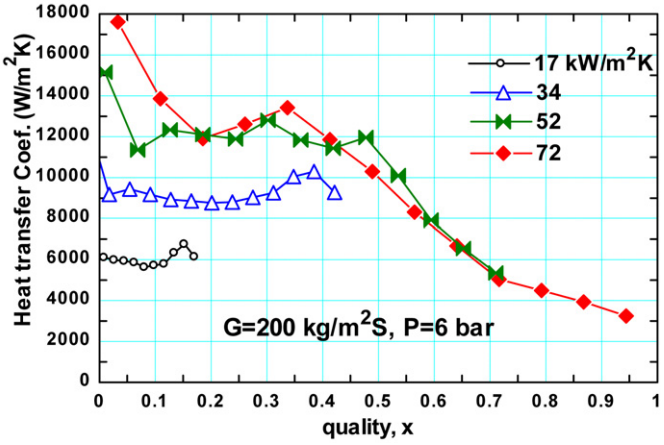

(a)

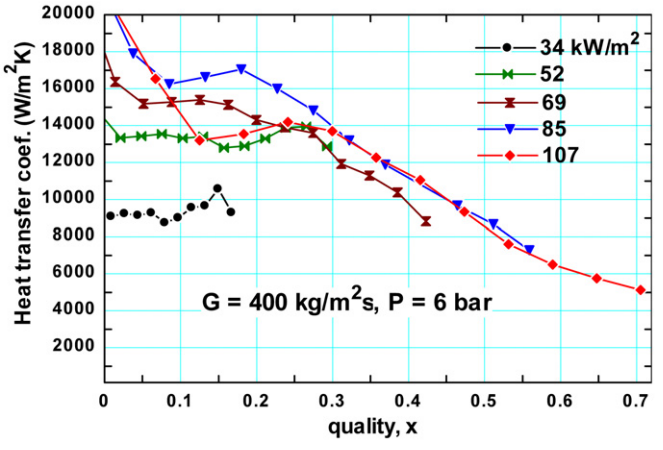

(b)

Fig. 6. Local heat transfer coefficient as a function of vapour quality with different heat fluxes at $P = 6$ bar: (a) $G = 200$ kg/m^2 s (b) $G = 400$ kg/m^2 s.

patterns observed in this experiment may not represent directly or exactly what is happening along the entire heated section, as these are taken at the exit of the tube and are subjected to any flow pattern development that may exist in the heated section.

Fig. 6 (a) and (b) depict similar curves to Fig. 5, but for a system pressure of 6 bar and mass flux of 200 and 400 kg/m^2 s,

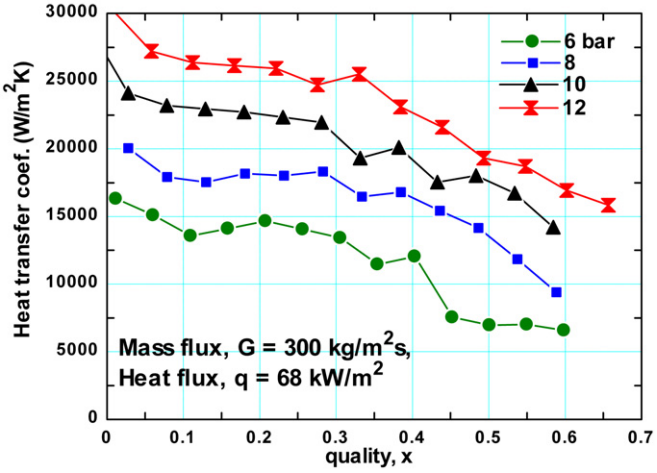

Fig. 7. Local heat transfer coefficient as a function of vapour quality for different system pressure, $G = 300$ kg/m^2 s, $q = 68$ kW/m^2.

respectively. Again at low heat flux values, when $x < \sim 0.5$ for $G = 200$ kg/m^2 s and $x < \sim 0.3$ for $G = 400$ kg/m^2 s, the experimental heat transfer coefficient is nearly independent of quality and dependent on heat flux. In the same range of quality, as the heat flux increases to the highest value of 107 kW/m^2, the heat transfer coefficient begins to decrease with heat flux. When the quality is greater than the above mentioned range, i.e. for ($x > \sim 0.5$ at 200 kg/m^2 s and $x > \sim 0.3$ for 400 kg/m^2 s) the heat transfer coefficient decreases with quality and becomes independent of heat flux.

The heat transfer coefficient is depicted as a function of system pressure in Fig. 7 for a mass flux of 300 kg/m^2 s and heat flux of 68 kW/m^2. The heat transfer coefficient increases with system pressure for the range of quality covered here, i.e. $x < 0.6$. The increase in heat transfer coefficient with increasing saturation pressure could be due to the fact that bubble departure diameter decreases as the system pressure increases. The bubble departure frequency also increases with increasing pressure, Sharma et al. [29]. Therefore, bubble growth and departure from the tube wall is faster at high pressure values for the same heat flux. In nucleate boiling, the disturbance caused by bubbles growing and escaping from the wall contributes significantly to the heat transfer rate [6]. Also, the effect of pressure on the specific heat of vaporisation and liquid density may be an additional cause.

The dependence of the heat transfer coefficient on mass flux is depicted in Fig. 8 for a heat flux of 69 kW/m^2 and 8 bar pressure. As seen in the figure, the heat transfer coefficient is almost independent of the mass flux.

5. Comparison with the model and discussion

In Figs. 9–11, the experimental measurements of local heat transfer coefficient as a function of quality are compared with the predictions of the three-zone model of Thome et al. [9], using the parameter values recommended by Dupont et al. [18]. Fig. 9 (a) and (b) depicts the effect of increasing heat flux at a pressure of 6 bar for mass fluxes of 200 and 400 kg/m^2 s, respectively. At low heat fluxes, the experimental heat transfer

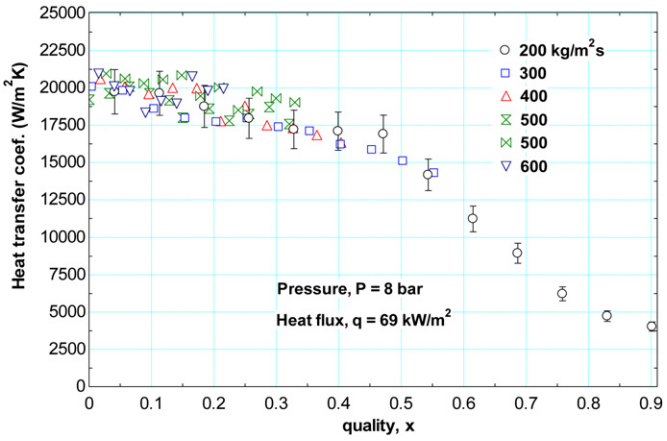

Fig. 8. Local heat transfer coefficient as a function of vapour quality for different mass flux, $P = 8$ bar, $q = 69$ kW/m^2.

coefficients increase with increasing heat flux; they are initially nearly independent of quality and then increase near the exit to the test section, e.g., $x > \sim 0.15$ at 34 kW/m^2. At higher heat fluxes, the coefficients have maximum values at the first measuring point that increase with increasing heat flux. Initially, they decrease with increasing quality, then remain fairly constant within the uncertainty limit. In this intermediate quality range, the dependence on heat flux is not straightforward: in Fig. 9(b), the heat transfer coefficients at 107 kW/m^2 fall below those at 69 and 85 kW/m^2. Beyond the fairly constant heat transfer coefficient region, the experimental points at all heat fluxes converge on a single line that decreases monotonically towards the test section exit. The predicted heat transfer coefficients exhibit simpler behaviour. They increase to a maximum around $x \sim 0.05$ to 0.1 for both mass flux values, then decrease monotonically with increasing quality. The coefficients are always higher than the experimental values at the higher heat flux. The three-zone model predicts heat transfer coefficients of the right magnitude, without a contribution from nucleate boiling, but it does not predict their independence of heat flux especially at high qualities. It is evident that further development of the model is required but it is not clear whether this should be fine-tuning of the convective mechanism or the inclusion of nucleate boiling. The predicted decrease in heat transfer with increasing quality is primarily due to the mechanism of periodic dryout and is sensitive to the parameter values for the thin liquid film. The experimental observations of decreasing heat transfer with increasing quality can be attributed to the mechanism of dryout. However, the local variation in the heat transfer coefficient before this stage at intermediate qualities could be related to transient dryout. There are also other possible explanations, including a decreasing effect of nucleate boiling or a local critical heat flux that may be different in the confines of a small tube from the critical heat flux in pool boiling. In these experiments, it was not possible to make local observations to confirm or exclude the occurrence of nucleate boiling.

As seen in Fig. 9(a), for mass flux 200 kg/m^2 s, at relatively low heat flux values, there is excellent agreement with the experimental values when $x < 0.5$. In Fig. 9(b), the model underpredicts the uniform heat transfer coefficient region for heat flux

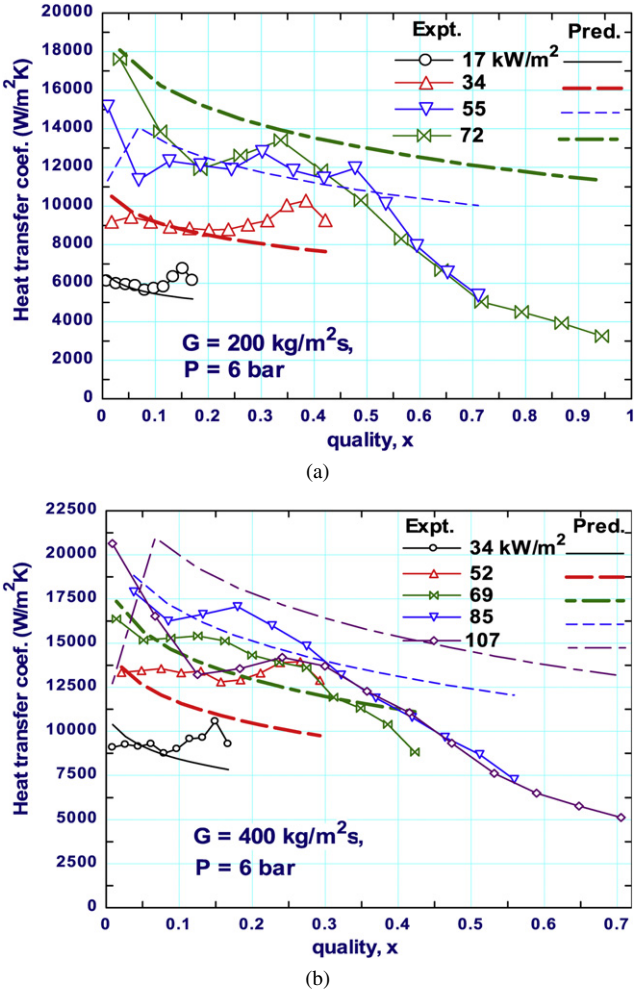

Fig. 9. Comparison between the local heat transfer coefficient predicted by the Thome et al. [9] model and the corresponding experimental results, $P = 6$ bar: (a) $G = 200$ kg/m^2 s, (b) 400 kg/m^2 s.

values of 52 and 69 kW/m^2. For mass flux of both 200 and 400 kg/m^2 s, at high heat flux values, the model over-predicts the experimental results, i.e. when $q > 72$ kW/m^2 for mass flux of 200 kg/m^2 s and $q > 85$ kW/m^2 for 400 kg/m^2 s, the experimental heat transfer coefficient tends to decrease with heat flux and what may be dryout begins early. However, the predicted heat transfer coefficient continues increasing with heat flux beyond the above limits.

In Fig. 9 (a) and (b), for heat flux $q = 55$ kW/m^2 and 107 kW/m^2, respectively, the experimental heat transfer coefficient is under-estimated at very low vapour qualities, near $x = 0$. This may be attributable to the onset of nucleate boiling, i.e. exclusion of bubble formation in the unconfined bubbly flow region in the model. The model assumes all-liquid flow up to the inception of the confined bubbles at $x = 0$ and employs a laminar fully developed single-phase heat transfer correlation that gives heat transfer coefficients much lower than that of unconfined bubbly flow region.

Fig. 10 compares the experimental and predicted effect of system pressure on the local heat transfer. The model predicted the lowest pressure $P = 6$ bar better than the rest. The trend with increasing system pressure is predicted correctly but the

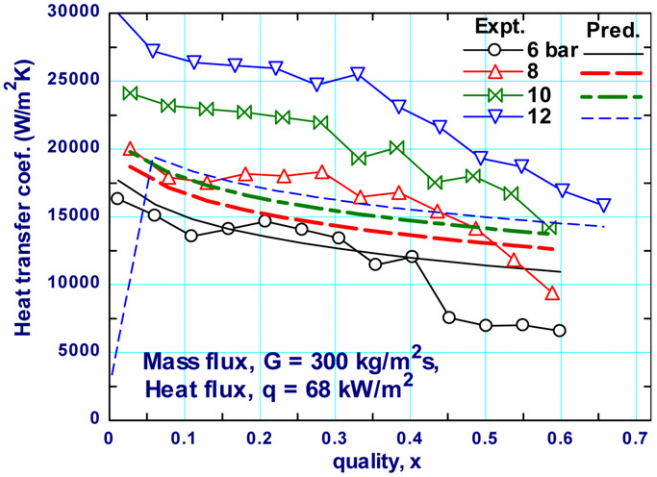

Fig. 10. Comparison between the effect of pressure predicted by the Thome et al. [9] model and the corresponding experimental results.

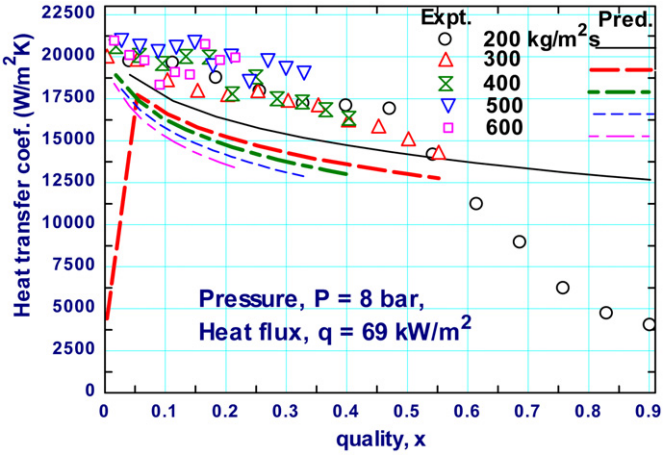

Fig. 11. Comparison between the effect of mass flux predicted by the Thome et al. [9] model and the corresponding experimental results.

magnitude of the change is greatly under-predicted. This could be attributed to a limitation of the one-dimensional model, which does not solve the equation of motion for the liquid slug. Also, looking at the model equations (7) and (8), the frequency should increase in a power law with pressure. However, the fact that the proportion of the time residence for the three different zones also depends on the liquid–vapour density ratio induces a counteractive effect. Therefore, one of the reasons for the diminishing effect of pressure on the predicted heat transfer coefficient could be that the density ratio, which decreases with pressure, tends to decrease the proportional time of the confined bubble regime, which has the larger heat transfer coefficient from the three zones. Hence, this has reduced the increase in pressure caused by the frequency increase.

It is noted above that there is no significant effect of mass flux on the experimental heat transfer coefficient. Fig. 11 presents the same curve as Fig. 8, now in comparison with the model prediction of a small decrease in heat transfer coefficient with increasing mass flux. The coefficients predicted by the convective model are only about 20% below the experimental values, which is a warning against interpreting independence of mass flux as an indication of the dominance of nucleate boiling.

6. Parametric sensitivity of three-zone model

As noted earlier, in the comparison with the model results, in all the above figures, the values used for the three parameters were those recommended by Dupont et al. [18]. Fig. 12 shows the effect of varying each of these parameters, while keeping the others as given by their respective Eqs. (6) to (9), on the predicted heat transfer coefficient for a sample case in which dryout appears to occur early at very low quality. Increasing the bubble generation frequency increases the predicted heat transfer coefficient by an amount that decreases with quality, Fig. 12(a). At very low quality (e.g., $x < 0.1$), a large increase in the frequency causes a sudden change in the character of the graph from a constant to a monotonic decrease. The frequency affects the relative contribution of the three zones using the respective residence times. This in turn affects the respective lengths of each zone (which also depend on local vapour quality), thereby changing the time-averaged heat transfer coefficient through the corresponding heat transfer coefficients of each zone. The sensitivity to the critical film thickness for dryout to occur, which is described as end film thickness in the model, is presented in Fig. 12(b). In the model, the dryout zone is directly linked to the value of the end film thickness. Increasing the end film thickness has an opposite effect on the heat transfer coefficient. In Fig. 12(c), the effect of changing the initial film thickness is depicted. Increasing the value increases the predicted heat transfer coefficient. Similar to the frequency curve, at higher initial film thickness, the curve changes its shape from monotonic increase to decreasing with quality at a low value of quality.

Fig. 12(d) presents the heat transfer predictions by the model when the end film thickness value (1.3 μm) is made almost equal to the measured average roughness of the tube (1.28 μm) and the other two parameters are modified, $C_{\delta 0}$ to 0.64 (2.2 times the standard value) and the frequency of bubble generation (f) to 1.75 times that recommended by Dupont et al. [18]. This results in a greatly improved prediction of a case in which dryout appeared to occur early at low quality.

In general, the three-zone model can be made to predict the 1.1 mm tube heat transfer results at low quality fairly well. The model has a great potential for further improvement because it includes a mechanism of periodic dryout. However, the decreasing heat transfer coefficients at high qualities near the exit of the test section, attributed to dryout, are not predicted well by the model. Moreover, the fact that the three parameters in the model were optimised based on a large experimental database means that the model is not completely general and any genuine deviation in the prediction results could be compensated by the selection of these values. Therefore, further study leading to the independent evaluation of these parameters is necessary to make the model self-sufficient. Other features of the model that may require modification were suggested in Shiferaw et al. [17].

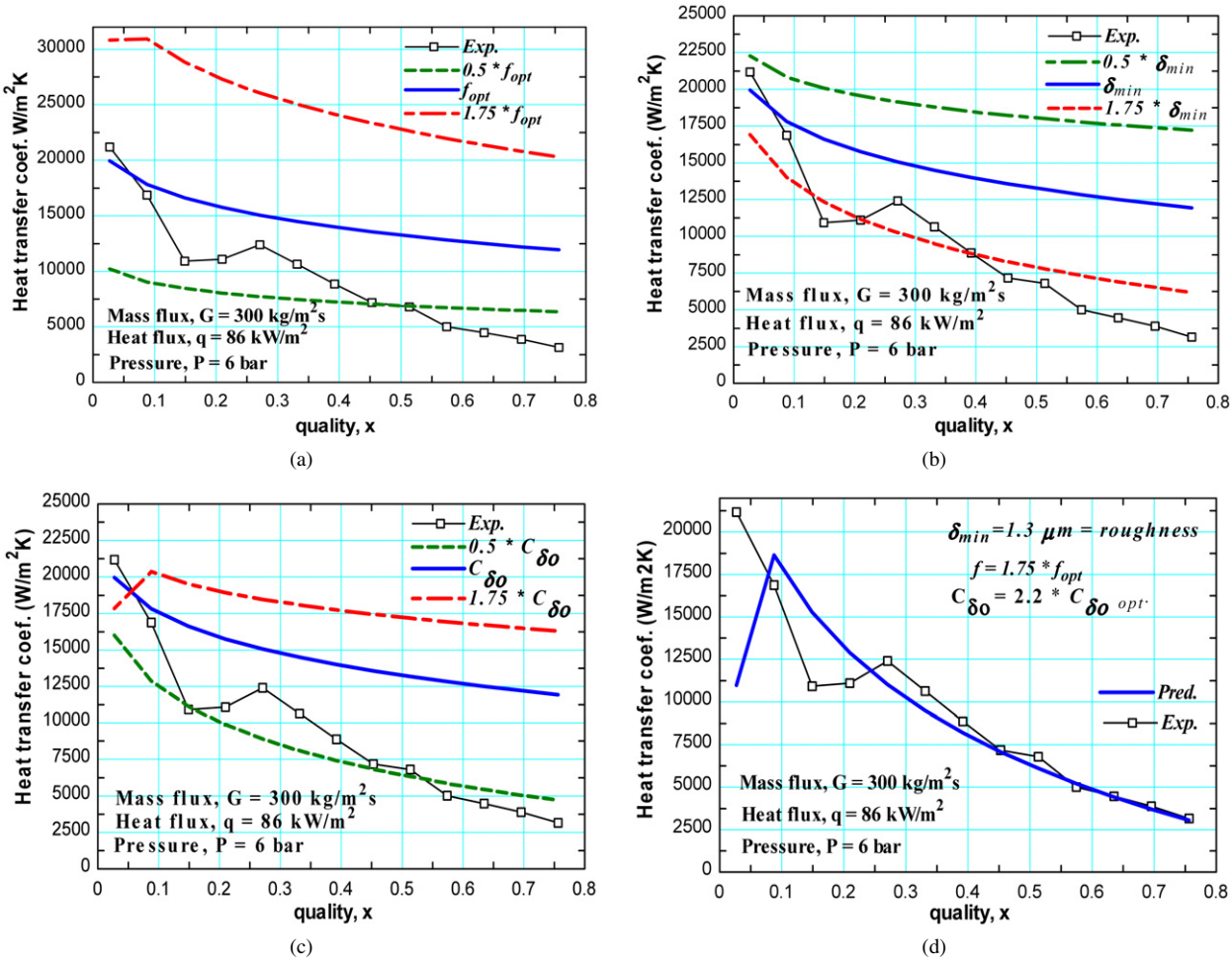

Fig. 12. Sensitivity of the heat transfer coefficient to the three optimised parameters given by the model: (a) frequency of bubble generation, (b) correction factor to the initial film thickness, (c) critical film thickness to dryout, (d) prediction of dryout when critical film thickness is same as roughness of the tube and the other two parameters are adjusted as shown.

7. Conclusions

Flow boiling experiments in a 1.1 mm tube inside diameter using R134a were conducted and the results were compared with the state-of-the-art three-zone evaporation model. The experimental results demonstrate that the heat transfer coefficient increases with heat flux and system pressure, but does not change with vapour quality when the quality is less than about 30 to 50%. This is conventionally interpreted as evidence that nucleate boiling is the dominant heat transfer mechanism in this vapour quality range. For vapour quality values greater than 50% and at high heat flux, the heat transfer coefficient does not depend on heat flux and decreases with vapour quality. This could be caused by partial dryout.

A detailed analysis of the three-zone evaporation model was presented in this paper based on current experiments. The model is based on convective heat transfer in the confined bubble regime, without any contribution from nucleate boiling. The model predicts fairly well experimental data that would be interpreted conventionally as nucleate boiling; especially the low pressure results. In its current form, the model over-predicts heat transfer in conditions in which dryout is thought to occur. The trend in the heat transfer coefficient with pressure changes is correctly predicted but the actual change is greater than that given by the model. Unlike the experimental results, the model shows a slight effect of mass flux on heat transfer coefficient. The model results are sensitive to the three parameters (bubble generation frequency, initial and end film thicknesses), which have to be optimised from experimental data. Some of the main important features of the model that may require modification include independent determination of the optimised parameters and an improvement of the partial dryout model.

References

[1] G.M. Lazarek, S.H. Black, Evaporative heat transfer, pressure drop and critical heat flux in a small vertical tube with R-113, Int. J. Heat Mass Transfer 25 (7) (1982) 945–960.

[2] M.W. Wambsganss, D.M. France, J.A. Jendraejczyk, T.N. Tran, Boiling heat transfer in a horizontal small-diameter tube, J. Heat Transfer 115 (1993) 963–972.

[3] T.N. Tran, M.W. Wambsganss, D.M. France, Small circular- and rectangular-channel boiling with two refrigerants, Int. J. Multiphase Flow 22 (3) (1996) 485–498.

[4] Z.Y. Bao, D.F. Fletcher, B.S. Haynes, Flow boiling heat transfer of Freon R11 and HCFC123 in narrow passages, Int. J. Heat Mass Transfer 43 (2000) 3347–3358.
[5] B. Palm, Mini-and microchannel research in Sweden, in: Proceedings of 1st ASME International Conference in Microchannels and Minichannels, Rochester, New York, 2003, pp. 25–31.
[6] X. Huo, Y.S. Tian, T.G. Karayiannis, R134a flow boiling heat transfer in small diameter tubes, in: Advances in Compact Heat Exchangers, R.T. Edwards, Inc., 2007, pp. 95–111 (Chapter 5).
[7] W. Qu, I. Mudawar, Flow boiling heat transfer in two-phase microchannel heat sinks-I. Experimental investigation and assessment of correlation methods, Int. J. Heat Mass Transfer 46 (2003) 2755–2771.
[8] W. Owhaib, B. Palm, Flow boiling heat transfer in vertical circular microchannel tube, Eurotherm seminar no. 72, Valencia, Spain, 31 March–2 April 2003.
[9] J.R. Thome, V. Dupont, A.M. Jacobi, Heat transfer model for evaporation in microchannels, Part I: Presentation of the model, Int. J. Heat Mass Transfer 47 (2004) 3375–3385.
[10] Y. Yan, D.B.R. Kenning, Pressure and temperature fluctuations during boiling in narrow channel, in: Eurotherm 62: Heat Transfer in Condensation and Evaporation, Grenoble, 1998, pp. 107–223.
[11] P.A. Kew, K. Cornwell, On pressure fluctuations during boiling in narrow channels, in: 2nd European Thermal-Science and 14th UIT National Heat Transfer Conference, Rome, 1996, pp. 1323–1327.
[12] L. Zhang, K.E. Goodson, T.W. Kenny, Silicon Microchannel Heat Sinks, Theories and Phenomena, Springer, Berlin, 2004 (Chapters 5–7).
[13] L. Zhang, E.N. Wang, K.E. Goodson, T.W. Kenny, Phase change phenomena in silicon microchannels, Int. J. Heat Mass Transfer 48 (2005) 1572–1582.
[14] S. Lin, P.A. Kew, K. Cornwell, Two-phase heat transfer to a refrigerant in a 1 mm diameter tube, Int. J. Refrigeration 24 (2001) 51–56.
[15] Y.Y. Yan, T. F Lin, Evaporation heat transfer and pressure drop of refrigerant R-134a in a small pipe, Int. J. Heat Mass Transfer 41 (1998) 4183–4194.
[16] D.S. Wen, Y. Yan, D.B.R. Kenning, Saturated flow boiling of water in a narrow channel: time-averaged heat transfer coefficients and correlations, Appl. Thermal Engrg. 24 (2004) 1207–1223.
[17] D. Shiferaw, T.G. Karayiannis, D.B.R. Kenning, A comparison with the three-zone model for flow boiling heat transfer in small diameter tubes, in: 13th International Heat Transfer Conference, Sydney, August 13–18, 2006, pp. BOI 16.
[18] V. Dupont, J.R. Thome, A.M. Jacobi, Heat transfer model for evaporation in microchannels, Part II: comparison with the database, Int. J. Heat Mass Transfer 47 (2004) 3387–3401.
[19] VDI-Warmeatlas, Springer-Verlag, Berlin, Heidelberg, 1997.
[20] V. Gnielinski, New equations for heat and mass transfer in turbulent pipe and channel flow, Internat. Chem. Engrg. 16 (1976) 359–368.
[21] S.W. Churchill, R. Usagi, A general expression for the correlation of rates of transfer and other phenomena, AIChE J. 18 (1972) 1121–1128.
[22] K. Moriyama, A. Inoue, Thickness of the liquid film formed by a growing bubble in a narrow gap between two horizontal plates, J. Heat Transfer 118 (1996) 132–139.
[23] M.G. Cooper, Heat flow rate in saturated nucleate pool boiling—a wide-ranging examination using reduced properties, in: Advances in Heat Transfer, vol. 16, Academic Press, Orlando, 1984, pp. 157–239.
[24] F.W. Dittus, L.M.K. Boelter, Heat transfer in automobile radiators of tubular type, Univ. California, Berkeley, Publ. Engrg. 2 (13) (1930) 443–461.
[25] B.S. Petukhov, Heat transfer and friction in turbulent pipe flow with variable physical properties, in: Advances in Heat Transfer, vol. 6, Academic Press, New York, 1970, pp. 503–564.
[26] T.G. Karayiannis, D. Shiferaw, D.B.R. Kenning, V.V. Wadekar, Flow patterns and heat transfer for flow boiling in small to micro diameter tubes, in: 5th Int. Conf on Transport Phenomena in Multiphase systems, Poland, June 30–July 3, 2008.
[27] L. Chen, Y.S. Tian, T.G. Karayiannis, The effect of tube diameter on vertical two-phase flow regimes in small tubes, Int. J. Heat Mass Transfer 49 (2006) 4220–4230.
[28] K. Cornwell, P.A. Kew, Boiling in small parallel channels, in: P.A. Pilavachi (Ed.), Energy Efficiency Process Technology, Elsevier Appl. Science, 1993, pp. 624–638.
[29] P.R. Sharma, A. Lee, T. Harrison, E. Martin, N. Krishina, Effect of pressure and heat flux on bubble departure diameters and bubble emission frequency, Grambling State University Technical report, 1996.